

## Modulated electron emission: The effect of elastic and inelastic electrons on core-level ionization

A. di Bona, G. C. Gazzadi, A. Borghi, and S. Valeri

*Istituto Nazionale per la Fisica della Materia and Dipartimento di Fisica, via Campi 213/a, 41100-Modena, Italy*

(Received 11 June 1997)

We investigated the elastic and inelastic contributions to the focusing and defocusing properties of low-index Fe atomic chains on keV electron beams. To this end, we measured the intensity of the  $2p$ -ionization loss signal from a thin Co film buried in a Fe matrix as a function of the incidence angle of the electron beam for different values of the beam energy. The angular anisotropy of the measured signal,  $A(z)$ , directly measures the focusing effect at the depth  $z$  where the Co marker is located. The maximum (102%) in  $A(z)$  occurs at  $z=5$  scatterers; at about 12 scatterers below the surface the anisotropy is still 86%. The intensity anisotropy of the  $2p$ -ionization loss we measured is compared to that of the Co *LMM* Auger signal and to single-scattering cluster calculations. It has been found that a finite spatial extension of the ionization region has to be taken into account to reproduce the experimental results. The relative weight of elastic and inelastic contributions to the  $2p$  core-level ionization cross section has been evaluated as a function of depth and electron energy. [S0163-1829(97)00645-0]

The basic mechanism leading to electron focusing along atomic rows in crystalline solids is the interference between the wave representing the electron beam (primary wave) and that scattered by the atomic potential. In the keV energy range the interference is constructive in the forward direction only, and thus the incident electron flux is effectively focused in a small angular range. This forward-focusing process provides the basis of several structural analytical techniques such as Auger/photoelectron diffraction and inelastic medium-energy electron diffraction; in these cases the primary waves are the Auger, photoemitted or backscattered electrons, respectively, and the scattering-interference process is experienced by the outgoing electrons,<sup>1-7</sup> leading to angular anisotropy in the emitted electron intensity.

When a collimated electron beam enters a solid, the incident wave flux is spatially modulated by the scattering-interference process, resulting in a marked dependence of the electron yield on the incidence angle [primary-beam diffraction modulated electron emission, (PDMEE)].<sup>8-11</sup> Beam electrons focused by the surface atoms give rise to strong maxims (about 10–15°, full width at half maximum) in the Auger and secondary emission as the incident beam aligns to the interatomic axes.

The anisotropy  $A$  (Ref. 12) of the electron wave along a given atomic row shows a characteristic dependence on the number of aligned atoms. The complex interaction between several structural (lattice constant, structure, temperature) and electronic (atomic specie, inelastic mean free path, etc.) parameters that determine the actual “anisotropy depth profile” or  $A(z)$ , has been investigated either theoretically or experimentally.<sup>9,13-23</sup>

In a solid, the incident wavefront hits about one thousand atoms per layer. Even in a single-scattering interpretation, the superposition of such a large number of scattered waves tends to cancel the focusing effect deep in the solid. Moreover, multiple-scattering (MS) calculations in Cu, Al, and Ge linear chains predict an effective defocusing even for a small number of scatterers, and a complete defocusing for six to eight atoms in the row.<sup>13,14</sup> Several experimental studies

have been done in order to get an insight into the anisotropy profile. The angular anisotropy of elastically scattered photoelectrons and their plasmon loss peaks along low index rows in Al, Ge, and W,<sup>15,16</sup> and the spot diameter in the secondary electron imaging patterns in the Pt[110] chain<sup>17</sup> have been monitored. A study of the focusing-defocusing effect as a function of depth along the [110] Ga chains in GaAs, GaP, and GaSb was performed by monitoring Ga Auger electrons and the related plasmon losses using PDMEE.<sup>18,19</sup> Direct experimental evaluation of the electron wave anisotropy along Ni and Fe chains was done using thin-film epitaxy.<sup>9,20-22</sup> The value of  $A$  and the defocusing length have both been found to be larger than theoretically predicted. The measured  $A(z)$  profile has been used to model the anisotropy of electron emission in ordered multilayers<sup>20</sup> or in alternate ordered/disordered layers.<sup>23</sup>

In electron-excited electron spectroscopy, the core-level ionization is produced by either the elastically scattered incident-beam electrons or the so-called backscattered energetic electrons, i.e., those electrons which undergo inelastic scattering before they produce a core-level hole. The inelastic electron field is less anisotropic than that of the elastically scattered electrons, depending on the amount of coherence they lose during the inelastic processes. The total ionization field is therefore determined by the superposition of the elastic and inelastic fields; thus the Auger signal anisotropy is determined by the relative weight of this superposition and by the energy dependence of the core-level ionization cross section as well. A definite separation between Auger electrons excited solely by the elastic or inelastic field is therefore impossible.

Fortunately, there are spectral features which originate from the elastic ionization field only, namely, the core-level ionization-loss peaks. Located at a fixed energetic distance from the elastic peak, they still permit a chemical identification of the atom from which they originate. These features have already been studied in the frame of a suitable comparison between incident beam and outgoing electron-diffraction experiments.<sup>24</sup> A comparison between the Auger and the

ionization-loss signals will enable us to separate the elastic and the backscattered contributions to the total ionization field.

In this study, we measured the elastic electron-beam anisotropy profile  $A(z)$  by monitoring the  $2p$  ionization loss and the  $LMM$  signals from a thin Co film used as a marker that was embedded in a Fe (001) matrix. By changing the depth at which the marker was located, we were able to sample  $A(z)$  from the surface to the maximum depth at which the signal coming from the marker could be detected. We found the best compromise between depth resolution, signal intensity, and analysis depth using a 3 ML-thick Co marker, that had been “virtually” moved by epitaxial Fe deposition up to 12 ML below the surface.

Sample preparation and scattering experiments were performed in a UHV system (base pressure  $<5 \times 10^{-11}$  mbar). The substrate was a Fe (001) single crystal that was cleaned by repeated sputter-annealing cycles.<sup>25</sup> Co and Fe were deposited in sequence by evaporation from wires, 99.99% purity, 1 mm diameter, heated by electron bombardment. The evaporated flux at the sample surface was about  $2 \text{ \AA}$  per min. During deposition, the pressure rose to  $5 \times 10^{-10}$  mbar. The Co film, 3 ML thick, was first deposited on the Fe substrate. Bulk Co has an hcp structure at room temperature, but it grows in a metastable bcc structure as a thin film on Fe (001); the bcc to hcp transition occurs for Co thicknesses larger than 20 ML (Refs. 24, 26–28) and is thus of no concern for our experiments. Subsequently, Fe was deposited over the Co film.

The basic idea in these experiments is to get a single-phase Fe bcc structure with an embedded Co marker, buried at different depths. The scattering factors of Fe and Co at keV energies are very similar, so that the electron beam sees a quasicontinuous and ordered structure, provided that the films grow in registry with the substrate. The quality of the epitaxial growth has been carefully checked at each deposition stage by low-energy electron diffraction analysis, PD MEE, and Auger electron spectroscopy. No evidence of disordered growth or deviation from a layer-by-layer growth have been observed.

Measurements were performed by a cylindrical mirror analyzer (CMA) working in the first derivative mode, with 0.6% resolution and 15 V peak-to-peak modulation. The coaxial electron gun was operated at 2.6 keV, 1  $\mu\text{A}$  over a  $0.1 \times 0.1 \text{ mm}^2$  area. An automated data-acquisition system rotates the sample in front of the analyzer and records the peak-to-peak intensity of the selected spectral features. We monitored the Co  $2p$  ionization loss and the Co  $LMM$  Auger peaks as a function of the beam incidence angle in a plane containing the [100] (surface normal) and the [010] directions. Measurements were also performed as a function of the primary beam energy, in the 1–3 keV range, for the Co film buried below 2 ML of Fe. The CMA was found to provide enough angular integration over the takeoff angle to prevent an outgoing electron-diffraction effect to be detected.<sup>8</sup>

The energy distribution spectrum of 3 ML of Co on Fe (001) is shown in Fig. 1, top panel, for a beam energy of 2.6 keV at normal incidence. The energy region of the Fe and Co L Auger series and of the  $2p$  ionization losses is shown. The intensities of the Fe  $2p$ , and Fe  $LMM$  signals as a function

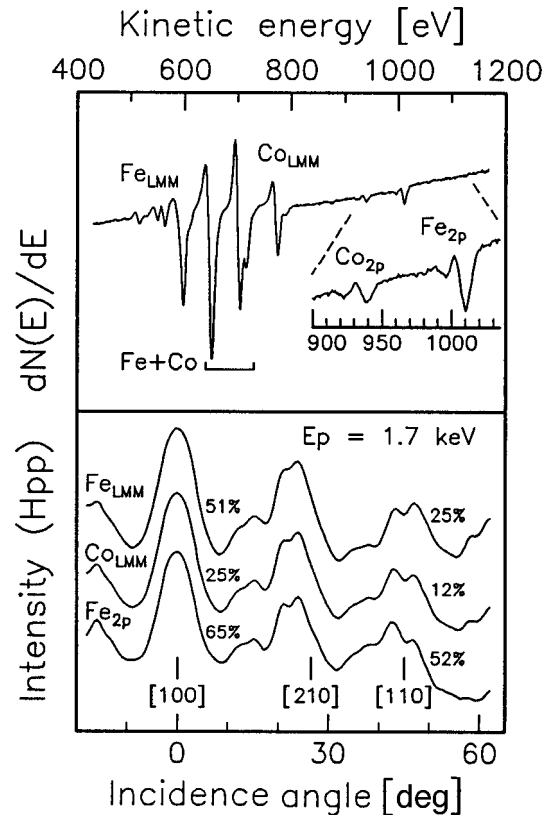


FIG. 1. Top panel: Energy spectrum of the electron emission from 3 ML of Co on Fe (001), for 1.7 keV electron beam at normal incidence. The ionization loss energy region is displayed in more detail. Bottom panel: angular dependence of the signal intensity of Fe  $LMM$ , Co  $LMM$ , and Co  $2p$  for a polar scan of the electron beam along the [010] azimuthal plane. The anisotropy values of the main forward focusing peaks are also indicated.

of the polar incidence angle along the [010] azimuth are shown in Fig. 1, bottom panel, for the clean Fe (001) surface. These two plots, as expected, are very similar because they both reflect the angular dependence of the electron-beam intensity at the atom sites. Forward-focusing features are detected at  $0^\circ$  and  $45^\circ$ ; these correspond to beam alignment along the [100] and [110] chains, respectively. Other peaks found between the main forward-focusing peaks are due principally to diffraction, although the maximum near  $25^\circ$  probably contain the forward-focusing contribution from the [210] incidence direction. The angular distribution of the Co  $LMM$  intensity from 3 ML of Co on Fe (100), also reported in Fig. 1, bottom panel, looks the same as the substrate signal, indicating that the overlayer grows in registry with the substrate. Despite these similarities, the strength of the intensity modulation (i.e., the anisotropy) is different for the three signals for reasons that will be discussed later on. The  $A$  values for the forward focusing features are reported in the figure.

The Co  $2p$ , and  $LMM$  signal anisotropy profile of the [100] forward-focusing feature excited by 2.6 keV electrons is shown in Fig. 2, bottom panel. The abscissa indicates the depth  $z$  at which the 3 ML Co marker film is located in the Fe matrix. As  $z$  increases, the Co  $2p$  signal intensity anisotropy sharply increases, reaches a maximum value of 102% at

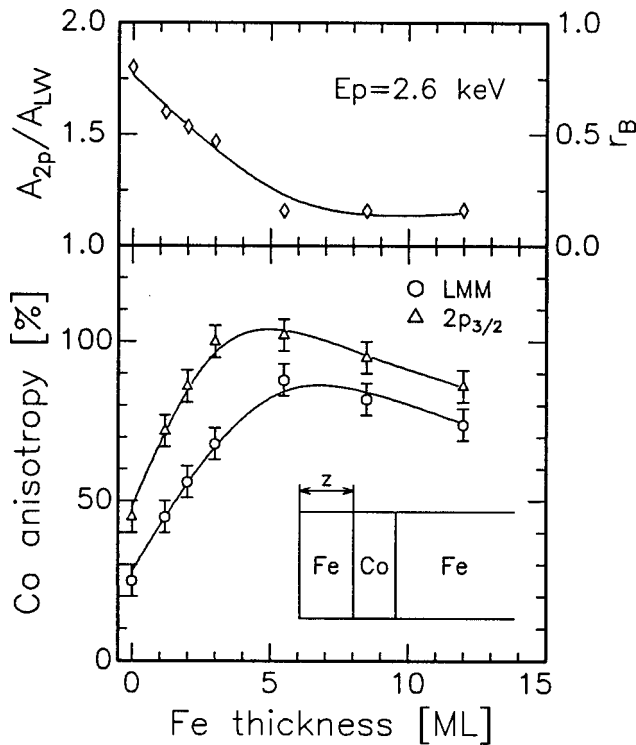


FIG. 2. Bottom panel: anisotropy depth profiles of the Co  $2p$  (triangles) and Co  $LMM$  (circles) signals from a 3 ML Co film embedded in a Fe matrix as a function of the depth the marker is located. The sketch at the bottom right hand indicates the experimental situation; the anisotropy value refers to the [100] focusing peak measured along the [010] azimuth. Top panel: ratio of the two signal anisotropies.

5 ML coverage, and then progressively reduces to 86% at 12 ML coverage. Since no inelastic contribution is expected in the ionization-loss signal, the Co  $2p$  anisotropy as a function of the Fe coverage, shown in Fig. 2, is representative of the  $A(z)$  profile induced by a 2.6 keV electron beam along the Fe [100] chain; the profile results from the competitive effects of focusing and defocusing processes.

The Co  $LMM$  Auger-signal anisotropy significantly deviates from that of the Co  $2p$  signal. The maximum value is smaller (85%) and occurs at a larger Fe coverage (7 ML). These differences are important in the low-coverage range, but are progressively smaller as the coverage increases. This is clearly shown in the upper panel, where the anisotropy ratio between the Co  $LMM$  and the Co  $2p$  emission is reported as a function of the Fe coverage. The ratio is a maximum at zero coverage (surface Co layer), decreases sharply in the 0–5 ML range, and then saturates at near unity at high coverage.

Generally speaking, the difference in the beam-energy dependence of the Auger and the ionization-loss signal intensities is due to several causes: (i) the kinetic energies of the measured signals are different as well as the corresponding inelastic mean free path (IMFP), so that the two signals originate from different regions of the  $A(z)$  profile; this point can here be disregarded because the Co marker localizes the emission at the same depth for both the  $2p$  and the  $LMM$  electrons, in spite of their different inelastic mean free path; (ii) contrary to the ionization loss, an appreciable fraction of

the Auger signal is excited by the inelastic ionization field, whose anisotropy is lower than that of the elastic field for the reasons we discussed above.

Actually, the ratio between the anisotropy of the ionization loss and the Auger signal  $r_A$ , is a measure of the so-called backscattering factor  $r_B$  in Auger microanalysis, i.e., the ratio between the total amount of ionization produced in the surface zone and that produced by the beam electrons alone.<sup>29</sup> If we assume that the inelastic ionization field is completely isotropic with respect to the incidence direction, then  $r_B = r_A - 1$ , otherwise  $r_B > r_A - 1$ .<sup>30</sup> The  $r_B$  scale is reported to the right of Fig. 2, upper panel.

The measured  $A(z)$  profile can be simulated by single-scattering cluster (SSC) calculations of the electron intensity at the atom sites. According to the SSC model, the total wave amplitude at a given position in the solid due to the incoming electron beam is calculated as the superposition of the primary wave (i.e., the incident beam) and a suitable number of (singly) scattered waves, each centered at the lattice sites. The actual beam intensity is then calculated as the squared module of the amplitude field. It is customary to calculate the scattered waves as a limited expansion on angular momentum eigenfunctions (about 40 partial waves for 2.6 keV energy). To account for the lattice vibrations and the inelastic attenuation, we used the Debye-Waller factors and the (IMFP), respectively.<sup>19</sup> We calculated the wave intensity along the [100] Fe atomic chains for normal and  $8^\circ$  off-normal (in the [010] azimuthal plane) beam incidence. From these two intensity fields,  $I_{\perp}(\mathbf{r})$  and  $I_{\parallel}(\mathbf{r})$ , which experimentally correspond to the maximum and minimum Co  $2p$  emission, respectively, we calculated the spatial distribution of the intensity field anisotropy around each emitting atom as  $A(\mathbf{r}) = 2[I_{\perp}(\mathbf{r}) - I_{\parallel}(\mathbf{r})]/[I_{\perp}(\mathbf{r}) + I_{\parallel}(\mathbf{r})]$ .

For the calculations we used about 500 scattered waves gathered in a cylindrical bcc cluster 15 Å in diameter and 35 Å height. The anisotropy profile  $A(z)$  was then calculated for values of  $z$  corresponding to the atomic positions. In Fig. 3 the results of the  $A(z)$  calculations, averaged over 3 layers to take into account the thickness of the Co marker, are compared with the experimental results. Curve ssc 1 refers to the beam intensity calculations at the atoms sites. Disregarding the absolute value of  $A(z)$ , its general behavior, i.e., the abscissa value for the maximum and the two different increase and decrease slopes, is quite nicely reproduced.

The assumption that the ionization probability of a given atom is proportional to the beam intensity evaluated at the corresponding lattice positions is rather simple and probably inaccurate. Due to the spatial extension of the core orbital, the interaction between the beam and the bound electron is not localized at the atom center, but depends on the matrix element of the electron-electron interaction between the initial state (actually the bound  $2p$  electron and the diffraction state) and the final state of the ionized atom (i.e., the ionized electron and the inelastically-scattered beam electron), whose exact determination goes beyond the scope of this paper. To include at least some aspect of the core orbital extension, we calculated the beam intensities and the corresponding anisotropy over a  $1.24 \text{ \AA}^3$  cubical volume centered around each emitting atom. The inset of Fig. 3 shows  $A(\mathbf{r})$  in a cut parallel to the surface plane passing through the center of an atom located 8.61 Å below the surface. The anisotropy

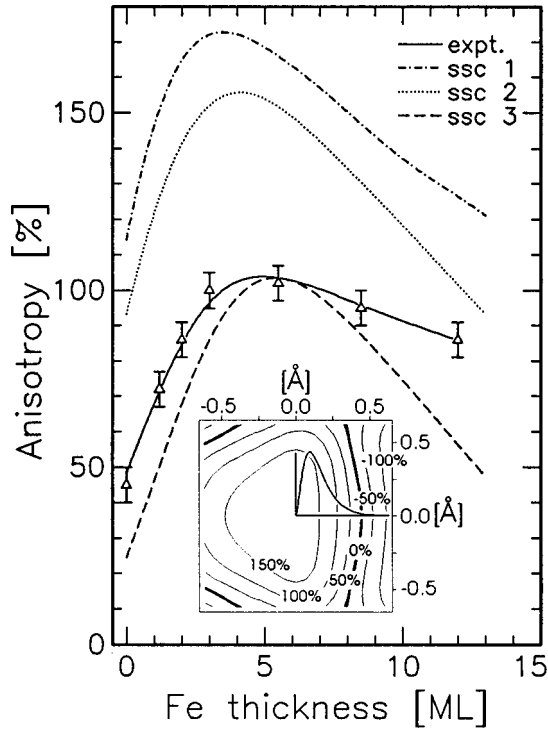


FIG. 3. Anisotropy depth profiles of the Co  $2p$  signals from a 3 ML Co film embedded in a Fe matrix as a function of the depth the marker is located; triangles are the experimental values, while dashed lines are the results of SSC calculations (see text for details). Inset: cut of the spatial distribution of the beam intensity anisotropy calculated over a  $1.24 \text{ \AA}^3$  volume centered around an atom located  $8.58 \text{ \AA}$  below the surface.

is not constant around the atom center. In particular, there are spatial regions where it is negative, i.e., where the electron beam is more intense at off-normal than at normal incidence. We spatially averaged  $A(\mathbf{r})$  assuming a weight function proportional to the squared modulus of the Co  $2p$  atomic radial function (curves ssc 2). The weight function represent a crude approximation of the ionization matrix element; nevertheless this approach effectively reduces the absolute value of the calculated anisotropy without changing its general behavior. In order to fit correctly the maximum value of  $A(z)$ , we also used a weight function that is unity within a sphere with radius  $0.6 \text{ \AA}$  (curve ssc 3).

Figure 3 clearly points out that SSC calculations overestimate the anisotropy value but, despite the crude assumptions of this theory, it correctly predicts a defocusing effect that is generally claimed to be correctly described only taking MS processes into account.<sup>14</sup> Furthermore, the predicted short MS defocusing length<sup>13</sup> clashes with the experimental results, which on the contrary agree with the SSC calculations.

We also investigated the effect of the incident electron energy on  $A(z)$ . The dependence of the intensity anisotropy on electron energy for the Co  $LMM$  and Co  $2p$  emission from 3 ML Co covered by 2 ML Fe is shown in Fig. 4. As the electron energy is raised from 1.2 to 3 keV, the Co  $2p$  intensity anisotropy increases, at a rate that progressively lessens. In contrast, the Co  $LMM$  anisotropy first increases very slowly, and then decreases significantly for electron en-

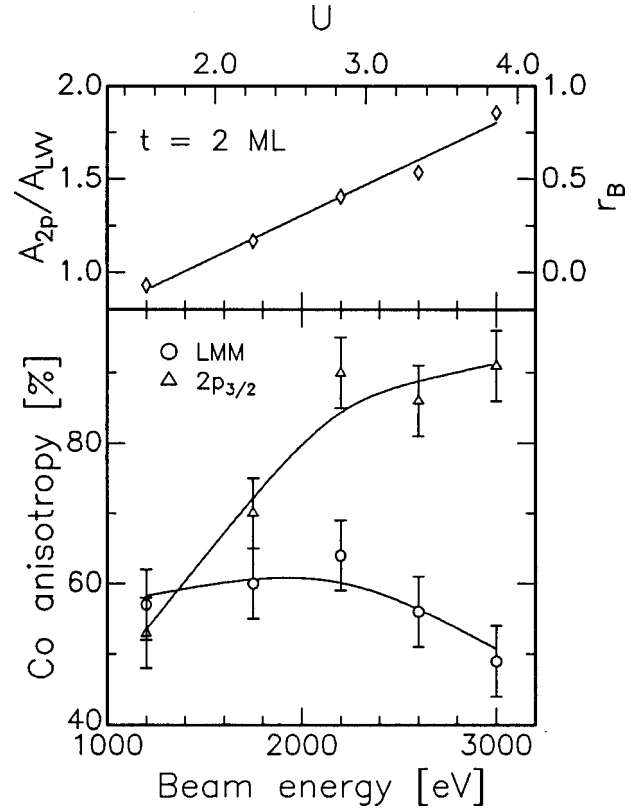


FIG. 4. Bottom panel: energy dependence of the anisotropy of the Co  $2p$  (triangles) and Co  $LMM$  (circles) signals from a 3 ML Co film located 2 ML below the surface of a Fe matrix; the anisotropy value refers to the  $[100]$  focusing peak measured along the  $[010]$  azimuth. Top panel: ratio of the two signal anisotropies.

ergies over 2.2 keV. The intensity anisotropy ratio between the Co  $LMM$  and the Co  $2p$  emission is reported in the top panel of Fig. 4. It is almost unity for an energy of 1.2 keV, near the ionization threshold of the  $2p$  core level, and then steadily increases as the primary beam energy increases; this fraction increases as the overvoltage ratio  $U$  (Ref. 31) increases and thus the anisotropy of the Auger signal is expected to decrease with the beam energy, as Fig. 4 shows.

In conclusion, we measured the  $A(z)$  profile along the  $[100]$  row of Fe (001) using thin film epitaxy of Co and Fe on Fe (001). Concerning the Co  $LMM$  Auger signal, we were able to separate the contribution of the primary beam electrons from that of the backscattered electrons. The backscattering factor  $r_B$  has been directly measured as a function of depth and beam energy. Single-scattering calculations agree very well with the experimental findings concerning the defocusing length, but they largely overestimate the absolute value of  $A(z)$ . An important improvement of the calculated behavior has been obtained by inclusion of the spatial extension of the core orbital, simulated by averaging the calculated anisotropy over a suitable weight function.

The authors are indebted to C. M. Bertoni for useful discussions. Financial support by the Ministero dell'Università e della Ricerca Scientifica e Tecnologica is gratefully acknowledged. The work of one of us (A.d.B.) is supported by Istituto Nazionale per la Fisica della Materia.

- <sup>1</sup>W. F. Egelhoff, Jr., Phys. Rev. B **30**, 1052 (1984).
- <sup>2</sup>Y. Gao and K. T. Park, Phys. Rev. B **46**, 1743 (1992).
- <sup>3</sup>W. F. Egelhoff, Jr., Crit. Rev. Solid State Mater. Sci. **16**, 213 (1990).
- <sup>4</sup>S. A. Chambers, Surf. Sci. Rep. **16**, 261 (1992); S. A. Chambers, I. M. Vitomirov, and J. H. Weaver, Phys. Rev. B **36**, 3007 (1987).
- <sup>5</sup>C. S. Fadley, in *Synchrotron Radiation Research: Advances in Surface Science*, edited by R. Z. Bachrach (Plenum, New York, 1992), Chap. 11; C. S. Fadley, Surf. Sci. Rep. **19**, 231 (1993).
- <sup>6</sup>D. P. Woodruff, Surf. Sci. **299/300**, 183 (1994).
- <sup>7</sup>B. L. Maschhoff, J.-M. Pan, and T. E. Madey, Surf. Sci. **258**, 190 (1991).
- <sup>8</sup>S. Valeri, A. di Bona, and G. C. Gazzadi, Surf. Interface Anal. **21**, 852 (1994).
- <sup>9</sup>S. Valeri, A. di Bona, and G. C. Gazzadi, Surf. Sci. **311**, 422 (1994).
- <sup>10</sup>S. Mroz and M. Nowicki, Surf. Sci. **297**, 66 (1993); A. Stuck, M. Nowicki, S. Mroz, D. Naumovic, and J. Osterwalder, Surf. Sci. **306**, 21 (1994).
- <sup>11</sup>M. V. Gomoyunova, S. L. Dudarev, and I. I. Pronin, Surf. Sci. **235**, 156 (1990), and references cited therein.
- <sup>12</sup> $A$  is defined as  $2(I_{\max} - I_{\min}) / (I_{\max} + I_{\min})$ , where  $I_{\max}$  and  $I_{\min}$  are the maximum and the minimum intensity in a small angular scan of the beam around the interatomic axis.
- <sup>13</sup>A. P. Kaduwela, D. J. Friedman, and C. S. Fadley, J. Electron Spectrosc. Relat. Phenom. **57**, 223 (1991).
- <sup>14</sup>H. A. Aebischer, T. Greber, J. Osterwalder, A. P. Kaduwela, D. J. Friedman, G. S. Herman, and C. S. Fadley, Surf. Sci. **239**, 261 (1990).
- <sup>15</sup>S. Hufner, J. Osterwalder, T. Greber, and L. Schlapbach, Phys. Rev. B **42**, 7350 (1990).
- <sup>16</sup>G. S. Herman and C. S. Fadley, Phys. Rev. B **43**, 6792 (1991).
- <sup>17</sup>M. Erbudak, T. Schulthess, and E. Wetli, Phys. Rev. B **49**, 6316 (1994).
- <sup>18</sup>S. Valeri, A. di Bona, and G. C. Gazzadi, Phys. Rev. B **50**, 14 617 (1994).
- <sup>19</sup>S. Valeri, G. C. Gazzadi, and A. di Bona, Phys. Rev. B **52**, 14 048 (1995).
- <sup>20</sup>S. Valeri, A. di Bona, and F. Borgatti, Surf. Sci. **371**, 143 (1997).
- <sup>21</sup>M. L. Xu and M. A. Van Hove, Surf. Sci. **207**, 215 (1989).
- <sup>22</sup>W. F. Egelhoff, Jr., Crit. Rev. Solid State Mater. Sci. **16**, 213 (1990).
- <sup>23</sup>S. Valeri, G. C. Gazzadi, A. Rota, and A. di Bona, Appl. Surf. Sci. (to be published).
- <sup>24</sup>S. Valeri, A. di Bona, G. C. Gazzadi, and F. Borgatti, J. Electron Spectrosc. Relat. Phenom. **76**, 723 (1995).
- <sup>25</sup>J. Kirschner, Surf. Sci. **138**, 191 (1984).
- <sup>26</sup>P. Boher, F. Giron, Ph. Houdy, F. Baudelet, A. Fontaine, J. M. Ladouceur, E. Dartyge, P. Beauvillain, C. Chappert, P. Veillet, and K. Le Dang, J. Appl. Phys. **71**, 1798 (1992).
- <sup>27</sup>J. Dekoster, E. Jedryka, C. Meny, and G. Langouche, Europhys. Lett. **22**, 433 (1993).
- <sup>28</sup>J. Zhang, Z.-L. Han, S. Varma, and B. P. Tonner, Surf. Sci. **298**, 351 (1993).
- <sup>29</sup>*Practical Surface Analysis*, edited by D. Briggs and M. P. Seah (Wiley, New York, 1990), 2nd ed., p. 202.
- <sup>30</sup>Let us assume  $I_A = I_P + I_B$ , where  $I_A$  is the intensity of the Auger signal, and  $I_P$  and  $I_B$  are the portions of it excited by the primary and the back-scattered electrons. The anisotropy of the Auger signal is therefore  $A_A = (A_P I_P + A_B I_B) / I_A$ , where  $A_P$  and  $A_B$  are the anisotropy of the primary and back-scattered ionization fields, respectively. If we assume  $A_P = A_{2p}$ ;  $A_A = A_{LMM}$  and  $A_B = 0$  then  $r_A \equiv A_{2p} / A_{LMM} = I_A / I_P \equiv 1 + r_B$  (Ref. 29).
- <sup>31</sup>In electron-excited ionization processes of a core level, the over-voltage ratio  $U$  is the ratio between the beam energy and the binding energy of the core level.